# Analysis of Performance of a Hot Gas Injection Thrust Vector Control System

R. Balu*
*Vikram Sarabhai Space Centre, Trivandrum, 695022 India*
and
A. G. Marathe,† P. J. Paul,‡ and H. S. Mukunda§
*Indian Institute of Science, Bangalore, 56012 India*

**The complex three-dimensional flowfield produced by secondary injection of hot gases in a rocket nozzle for thrust vector control is analyzed by solving unsteady three-dimensional Euler equations with appropriate boundary conditions. Various system performance parameters like secondary jet amplification factor and axial thrust augmentation are deduced by integrating the nozzle wall pressure distributions obtained as part of the flowfield solution and compared with measurements taken in actual static tests. The agreement is good within the practical range of secondary injectant flow rates for thrust vector control applications.**

## Nomenclature

$A$ = area of cross section
$a$ = sonic speed
$C_f$ = thrust coefficient
$e$ = total energy
$F$ = thrust
$H$ = conservative variables tensor
$I_{sp}$ = specific impulse
$K$ = jet amplification factor
$M$ = mach number
$\dot{m}$ = mass flow rate
$m_r$ = injectant flow rate ratio
$N$ = number of cells
$n$ = surface normal vector
$p$ = pressure
$p_r$ = injection pressure ratio
$Q$ = conservative variables vector
$R$ = gas constant
$r$ = radial coordinate
$S$ = surface area
$T$ = temperature
$T_r$ = injection temperature ratio
$t$ = time
$U$ = total velocity vector
$u, v, w$ = velocity in $x, y, z$ directions
$V$ = volume
$x, y, z$ = coordinate directions
$\alpha$ = $(\gamma - 1)$
$\beta$ = $\alpha/2\gamma$
$\gamma$ = ratio of specific heats
$\delta$ = main thrust deflection
$\varepsilon_i$ = injection angle
$\theta$ = circumferential coordinate
$\rho$ = density

*Subscripts*

$a$ = ambient
$i$ = injection
$n$ = normal
$o$ = stagnation state
$p$ = primary (rocket) flow
$r$ = radial direction
$s$ = secondary (side) jet
$w$ = wall
$x, y, z$ = in $x, y, z$ direction
1 = inlet section

Received Feb. 19, 1990; revision received June 20, 1990; accepted for publication June 25, 1990. 

*Head, Computational Fluid Mechanics Section.
†Assistant Professor, Department of Mechanical Engineering.
‡Assistant Professor, Department of Aerospace Engineering.
§Professor, Department of Aerospace Engineering.

## Introduction

CONTROL forces required to steer a rocket or a missile along a prescribed trajectory can be generated by deflecting the thrust vector propelling it. This deflection can be accomplished in a number of ways, such as gimballing the entire rocket nozzle or inserting jet vanes in the rocket exhaust. All of these systems require components that work efficiently in the high-temperature environment of the rocket exhaust and are invariably associated with axial thrust loss during vectoring. The technique of secondary fluid injection into the rocket nozzle as a means to obtain the forces for thrust vector control (TVC) has many advantages over other existing systems such as the fact that it requires no moving parts and it generates control forces without loss of axial thrust.[1] The injected jet can be produced by a separate gas generator or tapped from the main rocket motor itself. The secondary fluid injected into the primary gas flow produces complex pressure distribution on the nozzle wall, resulting in a net side force that is larger than the momentum of the secondary jet. In addition, due to the added mass into the nozzle, there is a substantial augmentation of axial thrust itself.

In this paper, an attempt has been made to simulate computationally the flowfield due to secondary injection of a hot gas into the rocket nozzle and to derive the performance of the TVC system in terms of injectant specific impulse and axial thrust augmentation.

## Existing Models of Secondary Injection

The secondary jet injected into the nozzle flow produces a complex flowfield. Figure 1 shows important features of this flowfield. The main flow is deflected through a small separation shock and then through a much bigger bow shock. The mixing, heat exchange, and acceleration of the secondary jet produces an asymmetric pressure distribution on the nozzle wall, resulting in a net side thrust. Earliest attempts to model secondary injection was made by Walker and Shandor.[2] They essentially used a linear model assuming small injectant flow rates and calculated the side force based on the influence

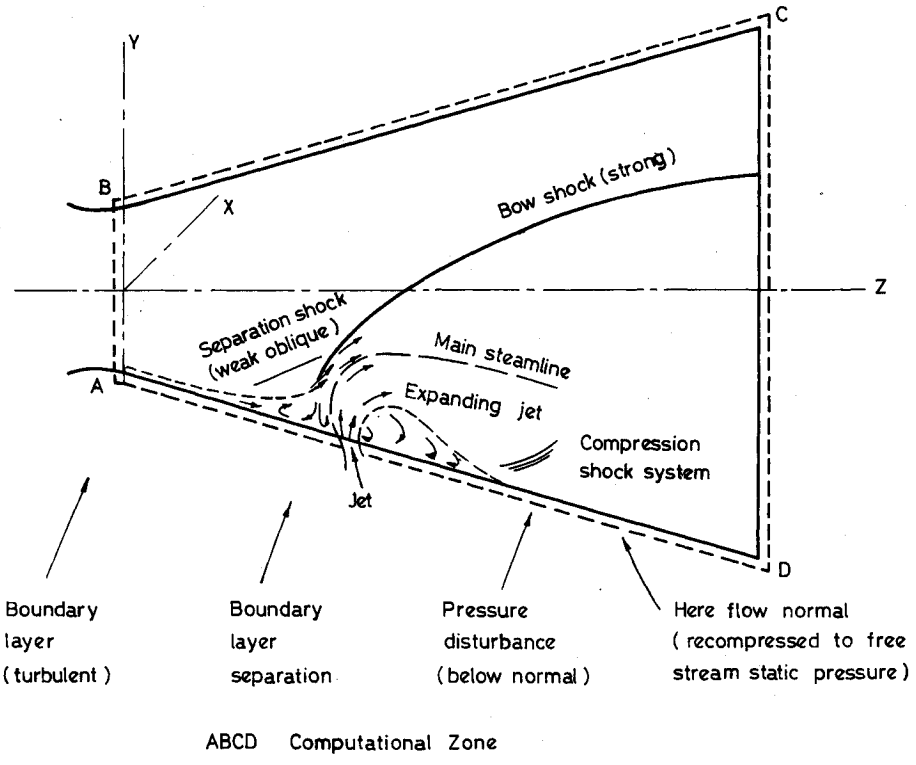


**Fig. 1 Schematic of salient features of secondary injection flowfield.**

coefficients proposed by Shapiro.[3] Since this theory is valid only for very small flow rates, it is useful only for comparing the relative merits of different injectants. In 1963, Broadwell[4] proposed the Blast Wave Analogy (BWA) to predict the side force due to secondary injection. This theory is based on the concept that the flowfield produced by secondary injection in a supersonic flow is analogous to the flowfield produced by the two-dimensional explosion of a line charge. The energy released by the explosion is set equal to the momentum of the secondary jet. The shape and strength of the resulting shock waves are approximated by the well-known solutions for a blast wave. Since the momentum of the secondary jet is considered as a gross parameter, the effect of important injection parameters, such as injection orifice size and geometry, injection pressure etc., cannot be accounted for by this model. Guhse[5] did experiments to demonstrate this lacuna. His experiments showed that these injection parameters had a significant effect on the side force, which the BWA failed to predict. Moreover, it predicts a linear variation of side force with injectant flow rate implying constant specific impulse of the injectant, whereas the experiments showed side force to be a highly nonlinear function of the injectant flow rate. The specific impulse is high at low flow rates of the injectant and it falls off rapidly at high flow rates. This feature, among other parameters such as the geometry of the separation zone, is mainly due to the fact that the side force produced by injection in a rocket nozzle is the resolved force on a plane passing through the nozzle axis and normal to the injection orifice. High forces induced away from the generator containing the injector will not, therefore, be effective for thrust vector control. This is referred to as cosine effect in the literature.[6] The existing theoretical models, in the absence of their ability to predict the complete three-dimensional pressure distribution, cannot account for this effect. An excellent review of all of the earlier attempts at modeling secondary injection TVC is given by Horton and Meade.[7]

## Present Approach

In the present work, an attempt is made to predict the pressure distribution generated by secondary injection by solving the unsteady three-dimensional Euler equations. An inviscid model is justified by the fact that the separation of the upstream boundary layer has a comparatively insignificant effect on the total side force, as shown by the experiments of Newton and Spaid.[8] It is observed in these experiments that a major contribution to side force comes from the pressure increase downstream of the injector under the bow shock. The contribution of the separated boundary layer to side force is small in case of thin turbulent boundary layer and supersonic main flow, typical conditions existing in rocket nozzles.

The governing equations are cast in integral conservation form, and an unsteady approach is used to compute the subsonic and supersonic regions of flow in an unified way. Since the injectant gas is also assumed to be hot gas taken from the main rocket motor itself, the effect of injection into the nozzle is considered simply as modification of nozzle wall boundary conditions in the injection zone. The governing equations are discretized using a finite volume concept, and the resulting difference equations are integrated in time using the explicit two level MacCormack's predictor—corrector scheme.[9] The equations are integrated until steady state is reached. The wall pressure distribution obtained as part of the solution is

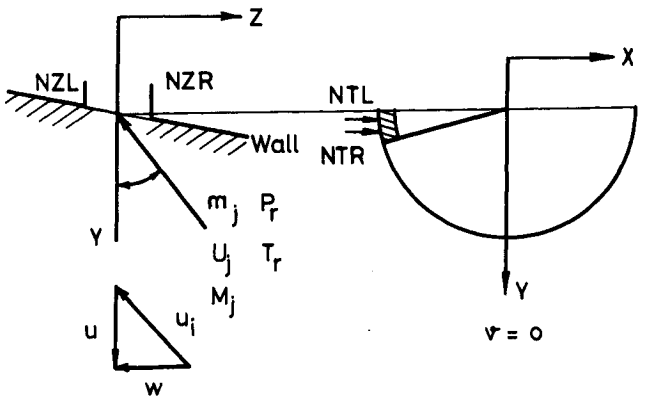


**Fig. 2 Boundary conditions at solid wall with secondary injection.**

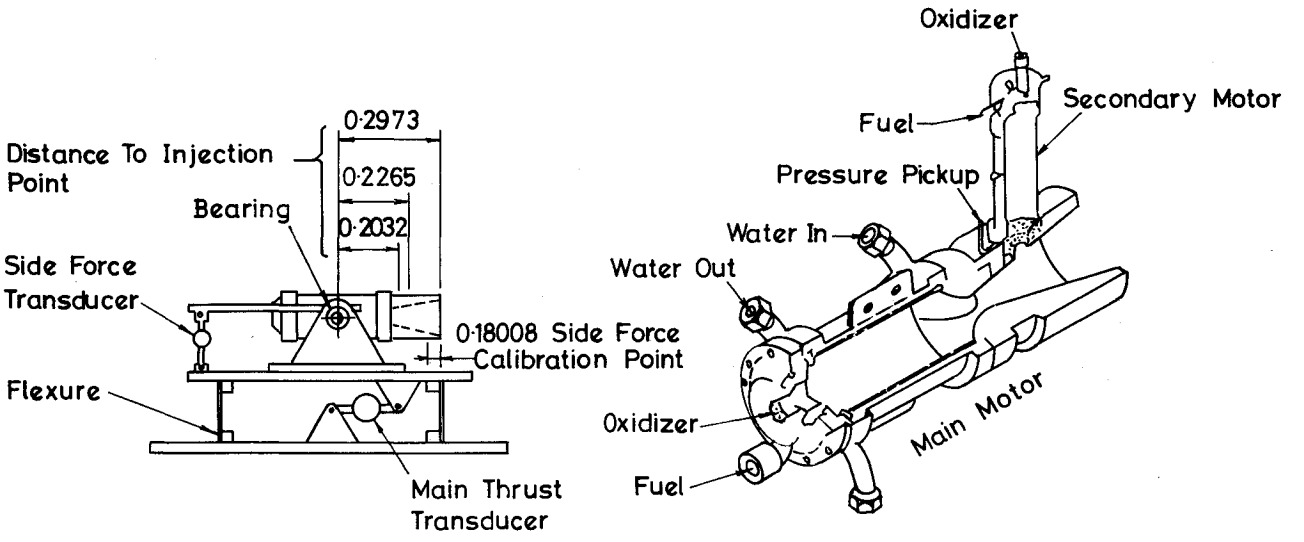


**Fig. 3 Schematic of test setup for hot gas injection TVC.**

integrated taking appropriate components in all of the three directions to get axial as well as side thrusts. Various overall system performance parameters such as jet amplification factor, injectant specific impulse, and axial thrust augmentation are calculated from the flowfield solution.

## Governing Equations and Boundary Conditions

The three-dimensional Euler equations in integral conservation law form after nondimensionalizing all of the velocities with adiabatic limiting velocity $a_o$, reference length $r_o$, and stagnation properties at inlet boundary can be written as

$$\frac{\partial}{\partial t}\iiint_v Q\,dv + \iint_s H(Q)\cdot ds = 0 \tag{1}$$

where

$$Q = [\rho, \rho u, \rho v, \rho w, e]^T \tag{2}$$

$$H_x(Q) = [\rho u, \rho u^2 + \beta p, \rho uv, \rho uw, (e + \alpha p)u]^T \tag{3}$$

$$H_y(Q) = [\rho v, \rho uv, \rho v^2 + \beta p, \rho vw, (e + \alpha p)v]^T \tag{4}$$

$$H_z(Q) = [\rho w, \rho uw, \rho vw, \rho w^2 + \beta p, (e + \alpha p)w]^T \tag{5}$$

The nozzle geometry is defined in a standard cylindrical ($z$, $r$, $\theta$) coordinate system. The entire computational domain is divided into $N_z$, $N_R$, and $N_T$ finite volume cells, in each of the coordinate directions, respectively. Ficticious cells are added at the boundaries to facilitate the implementation of boundary conditions. For the finite volume procedure, the surface area vectors of the cell faces and cell volume are needed and these are exactly computed from the geometry.

The secondary gas injection is done in the divergent section of the rocket nozzle, and, hence, constant supersonic flow conditions are imposed at the inlet boundary for simplicity. It may, however, be noted that, for more accurate computations, radially varying flowfield variables as obtained, for example, from a method of characteristic (MOC) solution could have been used as inlet boundary conditions. At the nozzle exit section (outflow boundary), the flow is again supersonic, and, hence, zero order extrapolation of all of the flow variables is used. Even with secondary injection, a single plane of symmetry exists and, hence, computations are done between $\theta = 0\ \pi$ in the circumferential direction. Symmetry conditions are imposed at these boundaries. At the nozzle wall, no mass flow condition is imposed, and, hence, the components of $H(Q)$ in Eqs. (3–5), become functions of pressure alone and are computed by extrapolation using three neighboring cells in the interior. In the injection zone, the boundary conditions are modified as follows.

The injection zone is identified by its bounding cell numbers NZL and NZR in the $z$ direction and NTL and NTR in the $\theta$ direction. If $\varepsilon_i$ is the injection angle, $p_r$ and $T_r$ are the ratio of stagnation pressure and temperature of the secondary to primary flows, and $M_i$ is the injection Mach number, then the conservative variables in the injection zone can be written as (Fig. 2),

$$(\rho u)_i = -(\rho U)_i \cos\varepsilon_i \tag{6}$$

$$(\rho v) = 0 \tag{7}$$

$$(\rho w)_i = -(\rho U)_i \sin\varepsilon_i \tag{8}$$

$$p_i = \left[1 + \frac{\alpha}{2}M_i^2\right]^{-\gamma/\alpha} P_r \tag{9}$$

$$e_i = p_i + \gamma\rho_i U_i^2 \tag{10}$$

where

$$(\rho U)_i = M_i\left[1 + \frac{\alpha}{2}M_i^2\right]^{\frac{-(\gamma+1)}{2\alpha}}\sqrt{\frac{\alpha}{2T_r}}\,P_r \tag{11}$$

With these boundary conditions, the governing equations are integrated from an initial specified flowfield at time $t = 0$. The integration time step is chosen to satisfy the Courant-

**Table 1 Hot gas injection TVC tests by Inoyue[10]**

| | |
|---|---|
| Test conditions | |
| Main Motor | |
| Propellant | RFNA/UDMH |
| Chamber pressure | 9.2 MPA |
| Nominal thrust | 17.8 KN |
| Nominal mass flow rate | 7.9 Kg $s^{-1}$ |
| Ratio of specific heats, $\gamma$ | 1.28 |
| Nozzle exit area ratio[2] | 12.00 |
| Injection Motor | |
| Propellant | RFNA/UDMH |
| Mass flow rate | 1.25 Kg $s^{-1}$ |
| Injector location | 0.46 |
| Injection Mach number | 1.00 |
| Injection angle | 0.0 deg |

**Table 2 Orifice size and location for various mass flow rates, $\theta_l = 0$ deg**

| $m_r$ | $A_i$ | $d_i$ | $Z_l$ | $Z_r$ | $\theta_r$ | $\frac{P_{os}}{P_{op}}$ |
|---|---|---|---|---|---|---|
| 0.030 | 9.87E-05 | 0.993E-02 | 0.0776 | 0.0875 | 0.12 | 0.392 |
| 0.045 | 1.67E-04 | 0.129E-01 | 0.0762 | 0.0891 | 0.136 | 0.314 |
| 0.070 | 2.76E-04 | 0.154E-01 | 0.0749 | 0.0903 | 0.186 | 0.347 |
| 0.100 | 3.64E-04 | 0.190E-01 | 0.0731 | 0.0921 | 0.230 | 0.329 |
| 0.180 | 8.38E-04 | 0.289E-01 | 0.0682 | 0.0971 | 0.310 | 0.239 |

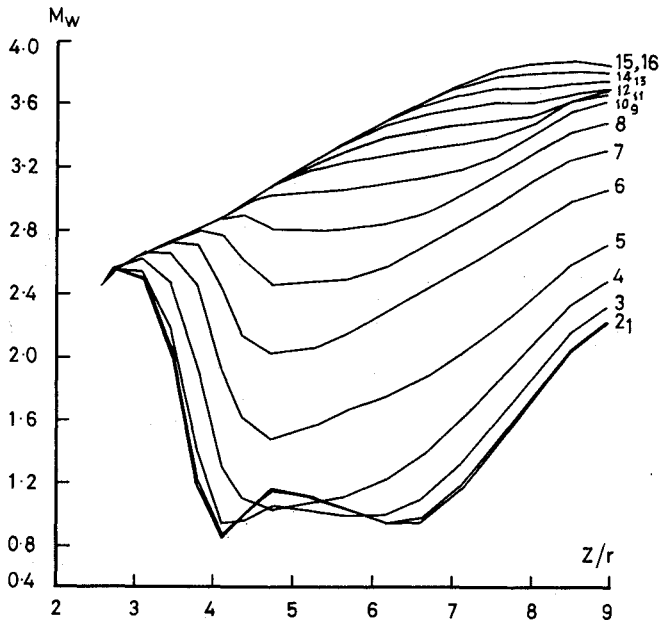


Numbers 1 To 16 Correspond To θ = 0·03, 0·091, 0·212, 0·393 0·574, 0·755, 0·936, 1·117, 1·298, 1·480, 1·710, 1·950, 2·223 2·407, 2·743 & 3·01

**Fig. 4 Axial distribution of wall Mach number for $m_r = 0.03$.**

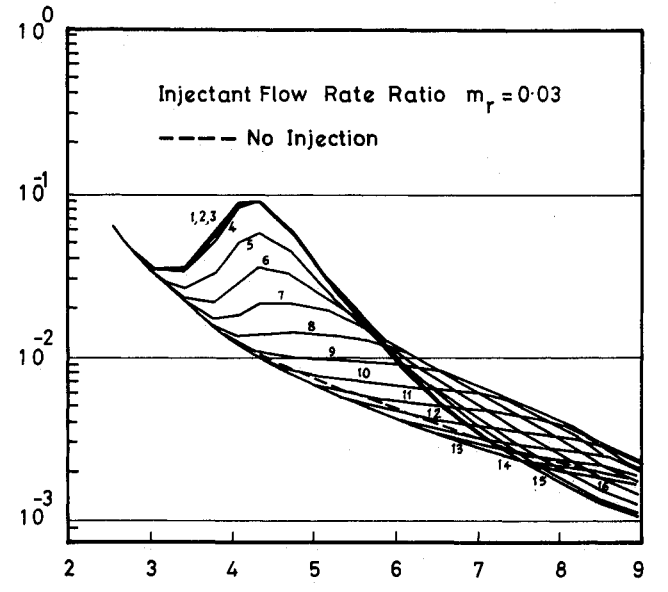


Numbers 1 To 16 Correspond To θ Values As In Figure-4

**Fig. 5 Axial distribution of wall pressure for $m_r = 0.03$.**

Friedricks-Lewy (CFL) stability criterion. The convergence is assumed to occur when the flowfield variables do not change by more than a prescribed tolerance. The variable considered for convergence in the present study is the change in pressure at all of the cells in the computational domain.

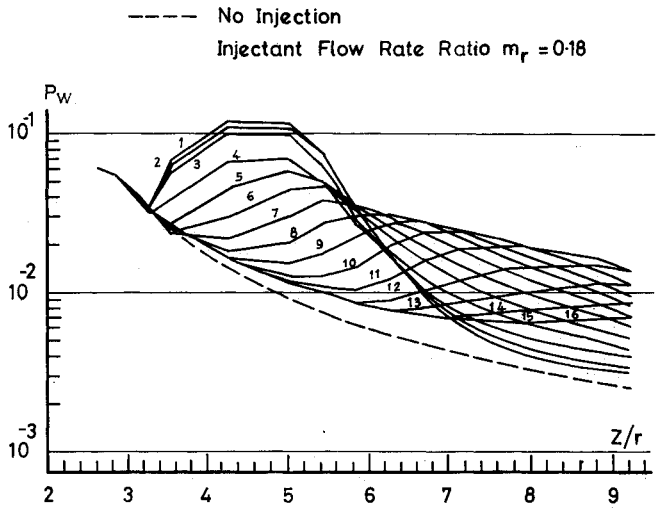


Number 1 To 16 Correspond To θ = 0·087, 0·262, 0·426, 0·578 0·733, 0·884, 1·031, 1·199, 1·349, 1·424, 1·701, 1·963, 2·275 2·487, 2·751, 3·01

**Fig. 6 Axial distribution of wall pressure for $m_r = 0.18$.**

## System Performance Predictions

The three-dimensional wall pressure distribution obtained as part of the solution is to be integrated by taking appropriate components of wall pressure both axially and circumferentially to get axial, normal, and side thrusts. The axial thrust is obtained by adding to the inlet momentum the contribution from wall pressure distribution along the nozzle contour up to the nozzle exit section. Thus, we have

$$C_f = \frac{F_p}{p_o r_o^2} = \frac{2\pi\gamma}{\alpha}\rho_1 A_1 U_1^2 + \int_{r_i}^{r_e}\int_0^{2\pi} \{P_w - P_a\} r_w \, dr_w \, d\theta + p_1 A_1 \quad (12)$$

$$C_{fs} = \frac{F_s}{p_o r_o^2} = \int_{Z_i}^{Z_e}\int_0^{2\pi} \{p_w - p_a\} r_w \cos\theta \, dz \, d\theta \quad (13)$$

$$C_{fn} = \frac{F_n}{p_o r_o^2} = \int_{Z_i}^{Z_e}\int_0^{2\pi} \{p_w - p_a\} r_w \sin\theta \, dz \, d\theta \quad (14)$$

The specific impulse ratio, which is the ratio of the injectant specific impulse and the main rocket motor specific impulse, is given by

$$K = \frac{C_{fs}}{C_f}\left[\frac{m_p}{m_s}\right] \quad (15)$$

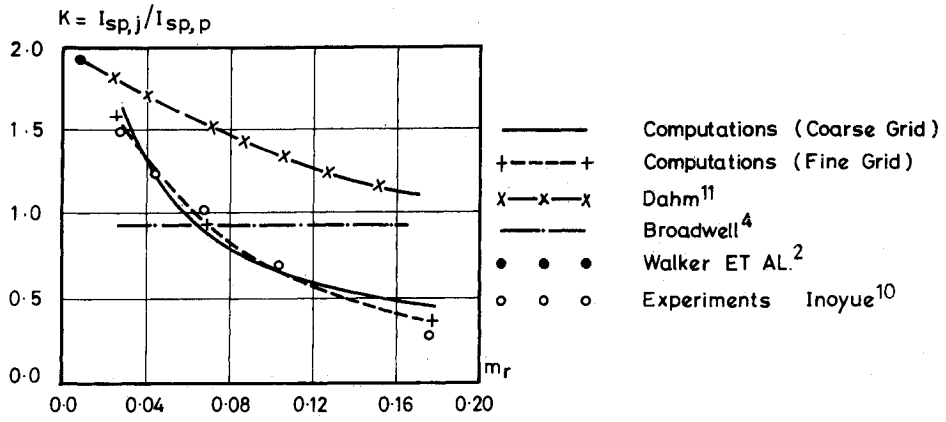


**Fig. 7 Comparison of predicted and measured specific impulse ratio.**

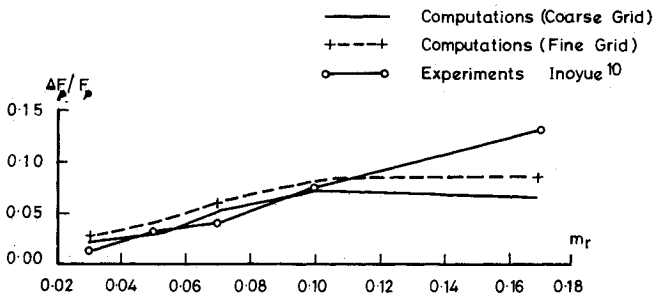


**Fig. 8 Comparison of predicted and measured axial thrust augmentation.**

and, finally, the main thrust deflection $\delta$ is given by

$$\delta = \tan^{-1}\left[\frac{F_s}{F_p}\right] = \tan^{-1}\left[\frac{C_{fs}}{C_f}\right] \tag{16}$$

## Results and Discussion

Using the approach just mentioned, the performance of the hot gas injection thrust vector control system experimented by Inoyue[10] has been analyzed. The side thrust and axial thrust were measured in these tests by load cell transducers, as shown in Fig. 3. The injectant was introduced into the rocket nozzle at a location 46% of the axial distance from the throat to the nozzle exit. The injection was sonic ($M_i = 1$) and was normal to the nozzle axis ($\varepsilon_i = 0$) through a single orifice. The injectant flow rate varied from 3 to 18% (nominal) of the main rocket motor nozzle flow. The main nozzle was conical with an exit area ratio of 12 and its wall profile is given by

$$r_w(Z) = 0.1 + 0.2673Z \tag{17}$$

Computations were performed for 3.0, 4.5, 7.0, 10.0, and 18.0% injectant flow rate on a coarse grid of 900 (10 × 9 × 10) cells and for 3.0, 7.0, and 18.0% flow rates on a fine grid of 4624 (17 × 16 × 17) cells. The test conditions and details of the main motor and the secondary motor are given in Table 1. Both the motors used unsymmetrical dimethylhydrazine/red fuming nitric acid (UDMH/RFNA) bipropellant. The extent of the orifice locations for different injectant mass flow rates and the injection conditions $p_r$ and $T_r$ are listed in Table 2. The inlet boundary conditions are taken corresponding to a Mach number of 2.21, and other flow variables are computed from stagnation (chamber) conditions using isentropic relations. The calculations were performed on the CYBER 170/730 computer system of Vikram Sarabhai Space Centre (VSSC), Trivandrum, India. The CPU times taken for a single mass flow case was about 90 min for the coarse grid and about 5 h for the fine grid. It was found that approximately 1500 time steps were necessary to reach convergence to steady-state solution. For calculations on the fine grid, the converged solution obtained on the coarse grid was used as an initial guess solution in order to reduce the computation time.

Figure 4 shows the wall Mach number distribution for 3% injectant flow. The Mach number becomes subsonic near the injection point. The flowfield along a diametrically opposite generator is seen to be relatively undisturbed and closely matched with that obtained from one-dimensional isentropic relations. Figure 5 shows axial pressure distribution at different circumferential locations. In confirmation with the experimental findings of Newton and Spaid,[8] the pressure in the wake of the injector falls below the undisturbed value, indicating overexpansion of the secondary jet. Near the injector, the wall pressure rises by more than three times the undisturbed static pressure. With increasing flow rates, this peak pressure increases only marginally, as is evident from Fig. 6, which shows the wall pressure distribution for 18% injectant flow. However, it is seen that the extent of the affected zone is increased markedly. The pressure distributions obtained have been integrated, as mentioned in a previous section, and the results are shown in Figs. 7 and 8. These results are also tabulated in Tables 3 and 4. Figure 7 shows the specific impulse ratio $K$ as a function of injectant flow rate ratio $m_r$ obtained from the present analysis with the experimentally measured values of Inoyue.[10] It is seen that the agreement is reasonable for the range of flow rates considered in the present study. The predictions from Broadwell's[4] BWA are also shown. The BWA predicts a constant specific impulse and,

**Table 3 Comparison of amplification factor, $K$**

| | $K_{\text{Theory}}$ | | |
|---|---|---|---|
| $m_r$ | Coarse grid | Fine grid | $K_{\text{Expt.}}$ |
| 0.0328 | 1.683 | 1.612 | 1.510 |
| 0.0444 | 1.330 | — | 1.300 |
| 0.0695 | 0.903 | 0.927 | 1.050 |
| 0.1028 | 0.643 | — | 0.660 |
| 0.1705 | 0.464 | 0.314 | 0.230 |

**Table 4 Comparison of axial thrust augmentation**

| | $(\Delta F_p/F_p)_{\text{Theory}}$ | | |
|---|---|---|---|
| $m_r$ | Coarse grid | Fine grid | $(\Delta F_p/F_p)_{\text{Expt.}}$ |
| 0.0328 | 0.021 | 0.030 | 0.0134 |
| 0.0444 | 0.027 | — | 0.0306 |
| 0.0695 | 0.051 | 0.061 | 0.0395 |
| 0.1028 | 0.070 | — | 0.0719 |
| 0.1705 | 0.061 | 0.082 | 0.1332 |

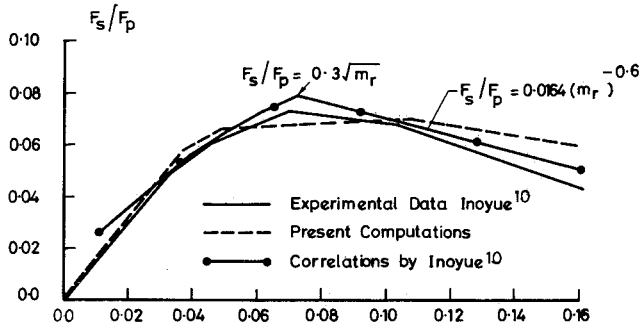


**Fig. 9 Comparison of predicted side force ratio with empirical correlations of Inoyue.[10]**

hence, constant $K$ with increasing flow rate. The predictions using the linearized model of Walker and Shandor.[2] is also shown in the figure, and the experimental as well theoretical estimations approach this limit as injectant flow becomes very small. Certain modifications to BWA have been introduced by Dahm,[11] and the predictions from his theory are also shown in Fig. 7. It is seen that, although a decreasing trend of $K$ with injectant flow rate is predicted, the predicted results are very much higher. [This may be due to the assumption of hypersonic flow ($M >> 1$) inherent in the Blast Wave Theory.] The predictions by the present analysis alone seems to follow the correct experimental behavior. It is also observed from the figure that the predictions from the fine grid solution agree better with the experiments, especially for flow rates higher than 10%.

Figure 8 shows the axial thrust augmentation as obtained from the present analysis with the experimental measurements. It is to be noted that none of the existing theories can predict this quantity as they cannot predict the three-dimensional pressure distribution with injection. The agreement between the present analysis and the experiments is quite good up to at least flow rates of 10%. Finally, the present results are compared in Fig. 9 with the empirical correlation proposed by Inoyue[10] in the form

$$\frac{F_s}{F_p} = C\left(\frac{m_s}{m_p}\right)^n \tag{18}$$

where $C$ and $n$ are constants. The agreement here, again, is very satisfactory.

## Conclusions

The various performance parameters of a hot gas injection thrust vector control system has been predicted by solving unsteady three-dimensional Euler equations and integrating the resulting wall pressure distribution. The results obtained in terms of gross system performance parameters agree quite well with experimental data. The existing analytical models are found to be incapable of correlating the experimental observations. The axial thrust augmentation due to secondary injection is also predicted by the present analysis and compares well with experimental measurements. The present analysis can be extended to two-phase flow, wherein the second phase can be liquid. With appropriate models for interphase mass, momentum, and heat transfer, predictions for liquid injection TVC can also be made.

## Acknowledgments

The authors wish to thank S. C. Gupta, Director, Vikram Sarabhai Space Centre, Trivandrum, India, for his kind permission to publish this paper.

## References

[1]Fruktow, N. N. et al., "Thrust Vector Control—Is it Keeping Pace?" American Society of Mechanical Engineers, Paper 62-AV-24, 1962.

[2]Walker, R. E., and Shandor, M. "Influence of Injectant Properties for Fluid Injection Thrust Vector Control," *Journal of Spacecraft and Rockets*, Vol. 1, No. 4, 1964, pp. 409–413.

[3]Shapiro, A. H., *The Dynamics and Thermodynamics of Compressible Fluid Flow*, Ronald, New York, 1954, Chap. 8.

[4]Broadwell, J. E., "Analysis of Fluid Mechanics of Secondary Injection for Thrust Vector Control," *AIAA Journal*, Vol. 1, No. 10, 1963, pp. 1067–1075.

[5]Guhse, R. D., "On Secondary Gas Injection in Supersonic Flow" *Journal of Spacecraft and Rockets*, Vol. 3, No. 1, 1966, pp. 143–149.

[6]"Solid Rocket Thrust Vector Control," NASA SP-8114, Dec. 1974.

[7]Horton, T. R., and Meade, A. J., "Thrust Vector Control of Rockets by Gaseous Injection. A Critical Appraisal of Theoretical Models," Rocket Propulsion Establishment, Westcott, England, Rept. RPE/67/7, July 1967.

[8]Newton, J. F., and Spaid, F. M., "Interaction of Secondary Injectants and Rocket Exhausts for Thrust Vector Control," *Journal of the American Rocket Society*, August 1962, pp. 1203–1211.

[9]MacCormack, R. W., "The Effect of Viscosity on Hypervelocity Impact Cratering," AIAA Paper 69-354, 1969.

[10]Inoyue, T. "Experiments on Rocket Thrust Vector Control by Hotgas Injection," *Journal of Spacecraft and Rockets*, Vol. 3, No. 4, 1966, pp. 737–739.

[11]Dahm, T. J., "The Development of an Analogy to Blast Wave Theory for Prediction of Interaction Force Associated with Gaseous Secondary Injection," VIDYA TN-9163, May 1964.